Results in Physics 35 (2022) 105377

Contents lists available at ScienceDirect

Results in Physics

journal homepage: www.elsevier.com/locate/rinp

A novel extended Gumbel Type II model with statistical inference and Covid-19 applications

Showkat Ahmad Lone [a,1], Tabassum Naz Sindhu [b,1], Anum Shafiq [c,1,*], Fahd Jarad [d,e,1,**]

[a] Department of Basic Sciences, College of Science and Theoretical Studies, Saudi Electronic University, (Jeddah-M), Riyadh-11673, Kingdom of Saudi Arabia
[b] Department of Statistics, Quaid-i-Azam University 45320, Islamabad 44000, Pakistan
[c] School of Mathematics and Statistics, Nanjing University of Information Science and Technology, Nanjing 210044, China
[d] Department of Mathematics, Faculty of Arts and Sciences, Cankaya University, 06530 Ankara, Turkey
[e] Department of Medical Research, China Medical University Hospital, China Medical University, Taichung 40402, Taiwan

ARTICLE INFO

Keywords:
NAPGT-II model
Mean square error
APT
Average Bias
Root mean square error

ABSTRACT

Statistical models play an important role in data analysis, and statisticians are constantly looking for new or relatively new statistical models to fit data sets across a wide range of fields. In this study, we used a new alpha power transformation and the Gumbel Type -II distribution to suggest an unique statistical model. The study contains a simulation analysis to determine the parameters' efficiency. Two real-life data sets were utilized to demonstrate the use of novel alpha power Gumbel Type II (NAPGT-II) distribution. NAPGT-II distribution yields a better fit than Weibull, new alpha power exponential, exponentiated Gumbel Type-II, Gumbel Type-II and exponentiated generalized Gumbel Type-II distribution, as evidenced by the data.

Introduction

The probability distribution plays a significant role in determining decisions under uncertainty. Their uses include reliability analysis, signal processing, and communication systems, as well as survival analysis and engineering. In the study of probability theory, it has been noted that conventional probability distributions fail to explain data with non-monotonic hazard functions. The Weibull model [1], for instance, fails to explain data with a bath-tub non-monotonic hazard shape. Over other accessible distributions, we can employ the Weibull, Exponential, and Gamma distributions to model the monotonic hazard rate. Such models are not rational or practical in the case of nonmonotonic hazard rates, like bathtub-shaped or upside-down bathtub-shaped hazard rates. There exist several data sets that exhibit a non-monotonic hazard rate function in practice. To describe these data, one must update the existing distribution, which can be employed to model both monotonic and non-monotonic hazard rate functions. Researchers are striving to improve existing distributions in order to solve this problem. The improvements are required by either increasing the number of parameters in the baseline distribution or creating a new mechanism for developing probability distributions.

In new research, the concept of generating new distributions by having an extra parameter to an existing family of distributions or mixing existing distributions has been a significant issue. It allows for a more adaptable distribution, providing for more complicated data structures to be modeled. Aldeni et al. [2], for instance, proposed a novel distribution family based on the quantile of the generalized lambda distribution. The T-normal family of models was investigated by Alzaatreh et al. [3]. The half-Cauchy family of models was introduced by Cordeiro et al. [4] with applicability to real-world phenomena. [5] proposed the concept of beta generated distributions, in which the parent distribution is beta and the foundation distribution is the cdf of any continuous random variable. [6] amended approach of [5] by switching Kumaraswamy distribution for beta distribution. There are several ways in the literature that may be utilized to improve the distribution broader and more adaptable so that the data can be modeled. One of the approaches available is Alpha Power Transformation (APT), which was recommended in [7]. They used the APT approach to generate the two-parameter alpha power Exponential (APE) distribution, which has a variety of features and implications. The investigators have recently attempted many generalizations of the APT approaches on modeling Weibull distributions [8,9]. Several scholars have used this transformation to create alpha power transformed distributions, including an APT generalized exponential distribution [10], APT inverse Lindly distribution [11], APT Lindly distribution [12], Alpha-Power

* Corresponding author.
** Corresponding author at: Department of Mathematics, Faculty of Arts and Sciences, Cankaya University, 06530 Ankara, Turkey.
E-mail addresses: anumshafiq@ymail.com (A. Shafiq), fahd@cankaya.edu.tr (F. Jarad).
[1] All authors have equal contribution.

https://doi.org/10.1016/j.rinp.2022.105377
Received 4 January 2022; Received in revised form 17 February 2022; Accepted 22 February 2022
Available online 5 March 2022

Pareto distribution [13], Ijaz et al. [14] suggested a novel family of distributions known as the Gull Alpha Power Family (GAPF).

In the scientific disciplines, extreme value models have risen to prominence as a statistical topic of research. Extreme point approaches are also gaining in popularity in a range of other domains. In extreme point studies, the likelihood of events that are more severe than those previously recorded must sometimes be calculated. In extreme value theory, the Gumbel distribution is a key distribution. It has a large capacity for use in the event of catastrophic disasters. It can also be applied to tables of life expectancy, hydrology, and rainfall. [15–19] provide additional information on Gumbel distribution.

Many generalizations of (GT-II) distributions have been developed in recent years to deal with various failure rates [20]. Adding more parameters to an existing distribution family is one such way. This research focuses on the new family of probability distributions which has proposed by Ijaz et al. [21], and employs the CDF of the GT-II distribution to establish its special form named novel alpha power Gumbel Type II(NAPGT-II) distribution. We have determined a number of statistical properties and specify how the suggested probability function can be used to both real and simulated data. Parameter estimation is fundamental when studying any probability distribution. For estimating the model's unknown parameters, we give classical approach. Check [20–24] for further details on a variety of classical estimation strategies.

The novel impact of current study using the APT approach to the Gumbel Type -II (GT-II) distribution is summarized as:

- The APT technique is a quick and easy way to add an extra parameters 'δ' to baseline distribution.
- The APT approach enriches and enhances the distribution.
- Both monotonic and non-monotonic hazard rates can be modeled using the APT approach.
- We get a better fit with the APT technique than with other modified models with the same or more parameters.
- To present an enhanced version of the GT-II distribution with a closed-form quantile function.
- To apply the maximum likelihood method to investigate the inferential properties of the NAPGT-II distribution, giving a thorough framework for practitioners.

New alpha power Gumbel Type II(NAPGT-II) distribution

The Novel Alpha Power Transformation (NAPT) family of probability distributions has recently presented by Ijaz et al. [21]. The distributions of the NAPT is stated as follows.

$$F_{NAPT}(t|\,\delta) = \delta^{-\log\left(\frac{1}{F(t)}\right)}, t \in \mathbb{R}, \delta > 0. \tag{1}$$

The PDF refers to (1) is

$$f_{NAPT}(t|\,\delta) = \frac{\log(\delta)\,\delta^{-\log\left(\frac{1}{F(t)}\right)} f(y)}{F(y)}, \delta > 0. \tag{2}$$

Ijaz et al. [21] developed the New Alpha Power Exponential (NAPE) model by using the cumulative distribution function of the Exponential distribution (ED) in (1). The new intended model is known as the new alpha power Gumbel Type II (NAPGT-II) by combining the alpha power transformed family of distributions and the Gumbel Type II distribution. The CDF and PDF of the Gumbel Type II (GT-II) model are accordingly given by

$$G(t|\,\lambda,\beta) = e^{-\lambda t^{-\beta}}, \lambda, \beta > 0, \tag{3}$$

and

$$g(t|\,\lambda,\beta) = \lambda\beta t^{-\beta-1} e^{-\lambda t^{-\beta}}. \tag{4}$$

Let T be a random variable that is continuous. Then, for the values $t > 0$, NAPGT-II is stated as

$$F_{\text{NAPGT-II}}(t|\,\Psi) = \delta^{-\lambda t^{-\beta}}, 0 < t < \infty, \lambda, \beta > 0, \delta > 1, \tag{5}$$

where $\Psi = (\lambda, \beta, \delta)$, λ is scale and δ, β are the shape parameters, accordingly. Here if we consider, $\delta = 1$, because $F_{\text{NAPGT-II}}(-\infty) = 1$, $F_{\text{MAPGT-II}}(+\infty) = 1$, and when $\delta < 1, F_{\text{NAPGT-II}}(-\infty) = \infty$, $F_{\text{NAPGT-II}}(\infty) = 1$, so in this study, we took $\delta > 1$. The PDF for (5) is as follows:

$$f_{\text{NAPGT-II}}(t|\,\Psi) = \lambda\beta t^{-\beta-1}\log(\delta)\,\delta^{-\lambda t^{-\beta}}, 0 < t < \infty, \lambda, \beta, \xi > 0, \delta > 1, \tag{6}$$

when $\delta = e$ we have Gumbel Type II (GT-II) distribution as a special case.

In the literature, terms like "failure rate function", is widely mentioned. This term is employed to indicate an element's failure rate over a given time period (t) and mathematically formulated as $h(t|\,\Psi) = f(t|\,\Psi)/[1 - f(t|\,\Psi)]$. The failure rate function is

$$h(t|\,\Psi) = \frac{\lambda\beta t^{-\beta-1}\log(\delta)}{\delta^{\lambda t^{-\beta}} - 1}, \tag{7}$$

is an ideal mechanism in reliability study. The chance that a component will survive at time t can be described as the reliability function $S(t|\,\Psi)$. Analytically, it is characterized as $S(t|\,\Psi) = 1 - f(t|\,\Psi)$, here, $S(t|\,\Psi)$ functions of NAPGT-II model is

$$S(t|\,\Psi) = 1 - \delta^{-\lambda t^{-\beta}}. \tag{8}$$

One of valuable reliability indicators is the cumulative hazard rate function (CHRF). The CHRF is a measure of risk: higher the $H(t|\,\Psi)$, elevate the risk of collapse by t -time.

$$H(t|\,\Psi) = \int_0^t h(y|\,\Psi)dy = -\log\left[S(t|\,\Psi)\right]. \tag{9}$$

$$H(t|\,\Psi) = -\log\left(1 - \delta^{-\lambda t^{-\beta}}\right). \tag{10}$$

Mills ratio is defined by $M(t|\,\Psi) = S(t|\,\Psi)/f(t|\,\Psi)$. Mills ratio of T is given by

$$M(t|\,\Psi) = \frac{\delta^{\lambda t^{-\beta}} - 1}{\lambda\beta t^{-\beta-1}\log(\delta)}. \tag{11}$$

The odd function is defined by $O(t|\,\Psi) = f(t|\,\Psi)/S(t|\,\Psi)$. The odd function of T is

$$O(t|\,\Psi) = \frac{1}{\delta^{\lambda t^{-\beta}} - 1}. \tag{12}$$

The $RHRf(t|\,\Psi)$ (reverse hazard rate function) is defined by $= f(t|\,\Psi)/f(t|\,\Psi)$. The RHRF of T is given by

$$RHRF(t|\,\Psi) = \lambda\beta t^{-\beta-1}\log(\delta). \tag{13}$$

Shape

Fig. 1 shows possible shapes for NAPGT-II density based on different parameter values. The potential shapes of the PDF corresponding to the parameter λ, that regulates the distribution's scale, as well as the two shape parameters δ and β, which govern the distribution's shapes, include growing, bathtub, symmetric, asymmetric, inverted U, decreasing, and inverted J forms. Fig. 1(a-i) demonstrate such shapes. Fig. 2(a-i) show failure rate function (FRF) shapes for the NAPGT-II model. The FRF forms, which include rising, U, increasing decreasing and bathtub shapes are shown in Fig. 2(a-i). These adaptable FRF shapes are appropriate for both monotonic and non-monotonic hazard rate behaviors, which are most common in real-time scenarios. Quantile function of NAPGT-II exhibits different types of forms (see Fig. 3).

Simulation

Hyndman and Fan [25] first proposed the notion of a quantile function ($t(k|\,\Psi)$. The kth QF of NAPGT-II is obtained by inverting the CDF (5). The NAPGT-II model can be easily simulated from (14). The generated variate having PDF (6) is

$$t(k|\,\Psi) = \left[-\frac{1}{\lambda}\left(\frac{\log(k)}{\log\delta}\right)\right]^{\frac{-1}{\beta}}, 0 < k < 1. \tag{14}$$

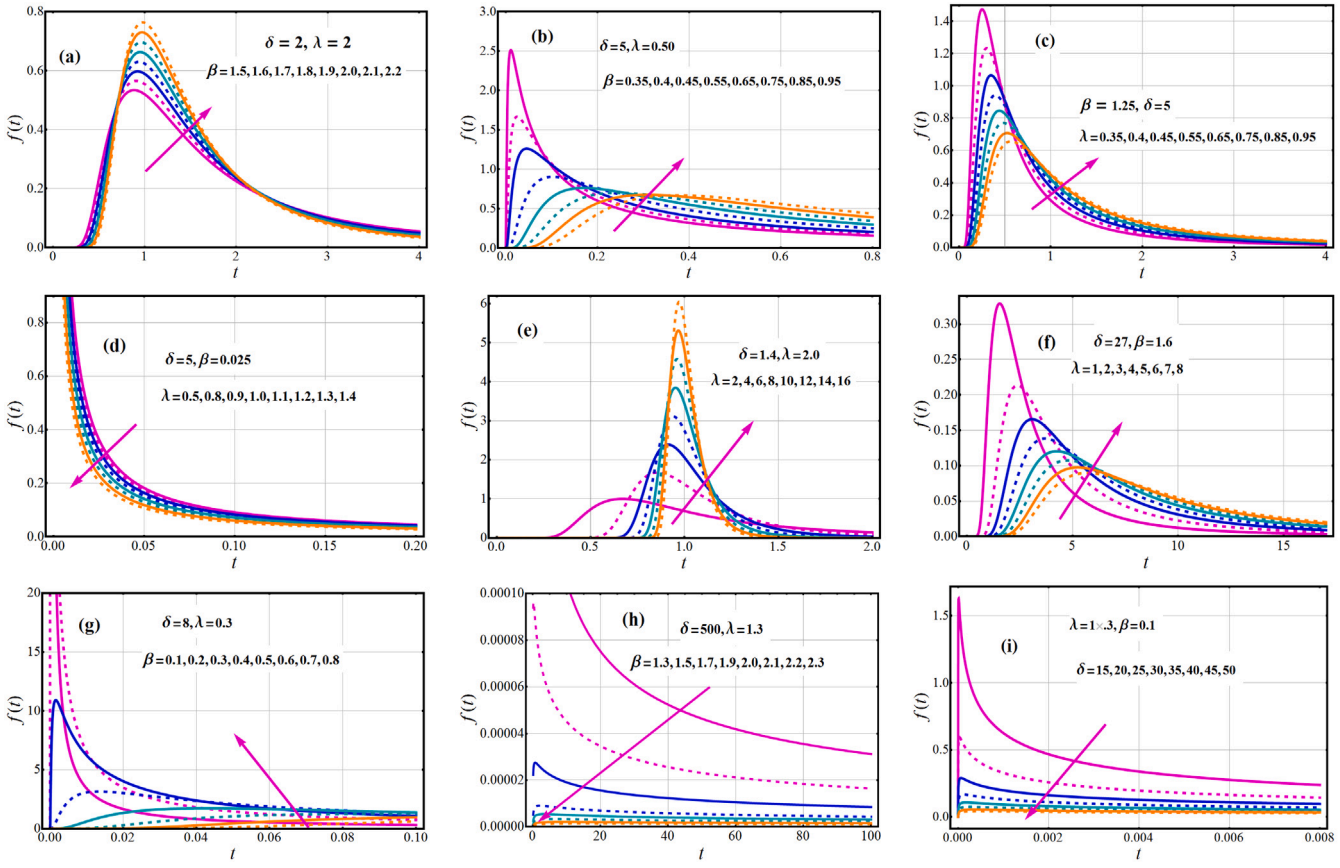

Fig. 1. Variations of PDF of NAPGT-II along with λ, δ and β.

As a consequence, the upper and lower quantiles, as well as the median, are computed as follows:

$$\tilde{T} = \left[-\frac{1}{\lambda}\left(\frac{-\log(2)}{\log\delta}\right)\right]^{\frac{-1}{\beta}}, \tag{15}$$

$$t(0.25|\Psi) = \left[-\frac{1}{\lambda}\left(\frac{\log(0.25)}{\log\delta}\right)\right]^{\frac{-1}{\beta}}, \tag{16}$$

$$t(0.75|\Psi) = \left[-\frac{1}{\lambda}\left(\frac{\log(0.75)}{\log\delta}\right)\right]^{\frac{-1}{\beta}}. \tag{17}$$

The differentiation of (14) provides the corresponding quantile density function

$$t'(k|\Psi) = \frac{-\left[\left(\frac{\log(k)}{\lambda\log\delta}\right)\right]^{\frac{-1}{\beta}}}{k\beta\log k}. \tag{18}$$

Skewness and Kurtosis

Eq. (14) with the following two formulas can be used to compute the Galton skewness coefficient, say S_Ψ, and Moors kurtosis, say K_Ψ, of the NAPGT-II distribution:

$$S_\Psi = \frac{Q(0.75|\Psi) - 2Q(0.5|\Psi) + Q(0.25|\Psi)}{IQR}. \tag{19}$$

and

$$K_\Psi = \frac{Q(0.875|\Psi) - Q(0.625|\Psi) + Q(0.375|\Psi) - Q(0.125|\Psi)}{IQR}. \tag{20}$$

These descriptive indicators, which are developed through quartiles and octiles, can offer more robust estimates than classical skewness and kurtosis metrics. Furthermore, S_Ψ and K_Ψ are less responsive to exceptions and perform better with inadequate moment models. At different levels of δ and ξ the QF and quantile density function layouts are shown in Fig. 4. The density of QF is noticed to be positively U shaped. Fig. 5 shows three-dimensional plots of possible S_Ψ and K_Ψ shapes for various values of Ψ. Fig. 5 also shows three-dimensional visualizations of the median function at various levels of δ. The stronger the change in the median curve, the lower the inputs of the parameter β and all potential values of β. Also, when the β approaches 1.3, the median function provides increasing values. On the other hand there is a noticeable shift in the skewness trend along β at lesser characteristics of β, but as β rises, it comes up to nearly 0.4. As β increases, the extent of peakedness of the model decreases and may also be platykurtic.

Mode

For determining the specified model's mode. To proceed, we calculate first derivative of the PDF (6) with respect to t and then equating this equation to zero as follows:

$$f'(t) = \frac{d}{dt}\left(\lambda\beta t^{-\beta-1}\delta^{-\lambda t^{-\beta}} Log[\delta]\right) = 0, \tag{21}$$

$$t^{-\beta-2}(-1-\beta)\beta\delta^{-t^{-\beta}\lambda}\lambda\log[\delta] + t^{-2-2\beta}\beta^2\delta^{-t^{-\beta}\lambda}\lambda^2(\log[\delta])^2 = 0. \tag{22}$$

Hence above equation yields the following result:

$$t \to e^{-i\frac{\pi}{\beta}}\beta^{\frac{2}{\beta}}\lambda^{\frac{2}{\beta}}(\log[\delta])^{\frac{2}{\beta}}\left(-\beta\lambda\log[\delta] - \beta^2\lambda\log[\delta]\right)^{-\frac{1}{\beta}}. \tag{23}$$

After considering the real value by using Euler's formula, we have a mode of NAPGT-II model as the following

$$t \to \cos\left(\frac{\pi}{\beta}\right)\beta^{\frac{1}{\beta}}\lambda^{\frac{1}{\beta}}(\log[\delta])^{\frac{1}{\beta}}(-1-\beta)^{-\frac{1}{\beta}}. \tag{24}$$

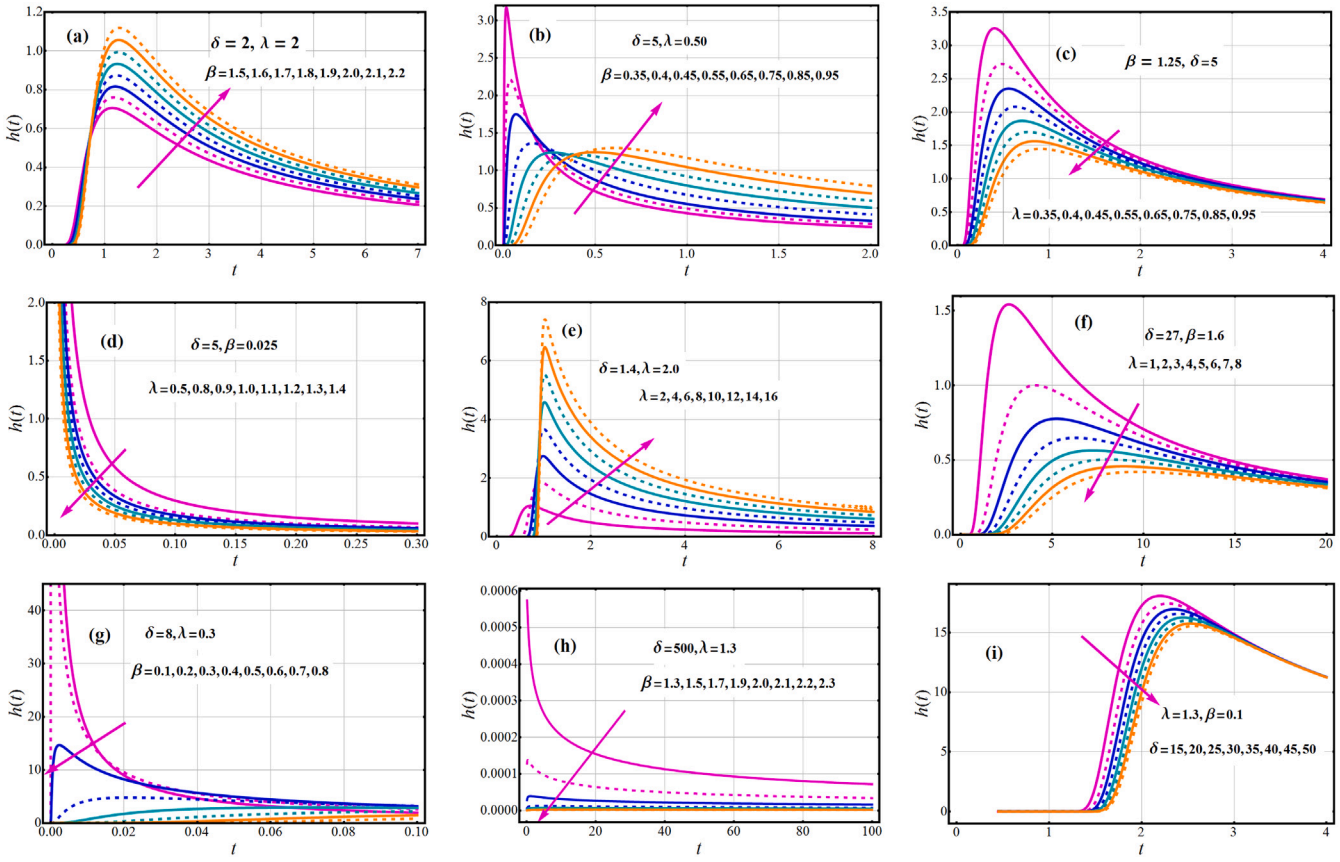

Fig. 2. Variations of FRF of NAPGT-II λ, δ and β.

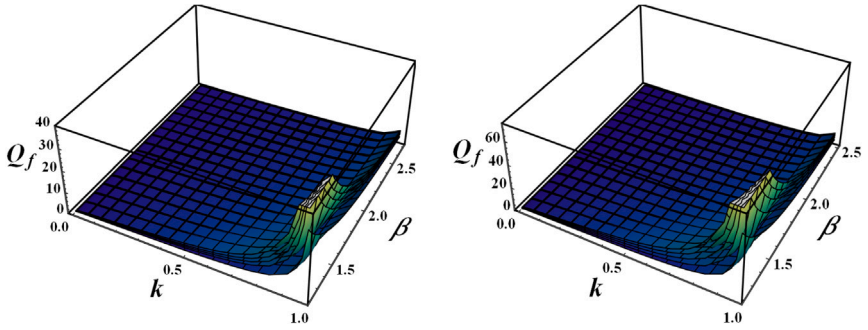

Fig. 3. Variations of QF of NAPGT-II with β and k at different extents of δ with $\lambda = 0.9$ (left), and QF of NAPGT-II with β and k at different extents of δ and $\lambda = 1.9$ (right).

Moments

Moments are utilized in statistics to explain the different features of a model. The central tendency, skewness, dispersion, and kurtosis of the model can all be examined using moments. If $T^{\sim}$ NAPGT-II(Ψ), then $n-$th moment $\acute{\mu}_n$ of T is

$$\acute{\mu}_n = \int_0^{\infty} t^n dF_t(t|\Psi); n = 1, 2, \ldots \tag{25}$$

In fact, we have

$$\acute{\mu}_n = \int_0^{\infty} t^n \lambda\beta t^{-\beta-1} \log(\delta)\, \delta^{-\lambda t^{-\beta}} dt; n = 1, 2, \ldots \tag{26}$$

let $\lambda t^{-\beta} = z$, then $-\beta\lambda t^{-\beta-1} dt = dz$, and using the series expression in the above equation $\alpha^{-\rho} = \sum_{k=0}^{\infty} \frac{(-1)^k (\log\alpha)^k}{k!} (\rho)^k$. As a result, the n^{th} order moment can be computed as,

$$\acute{\mu}_n = \sum_{k=0}^{\infty} \frac{(-1)^k (\lambda)^{\frac{n}{\beta}}}{k!} \left[\log(\delta)\right]^{k+1} \int_0^{\infty} z^{k-n/\beta} dz; n < \beta; n = 1, 2, \ldots \tag{27}$$

The integral (27) is convergent for $n < \beta$ otherwise it is divergent. The moment formula (27) can help us come up with some valuable statistical metrics. In (27), for example, the mean of T follows with $n = 1$. The negative moment of T can be simply determined by substituting n with $-\tau$ in (25).

Remark 1. The Moment Generating Function (MGF) is commonly employed in model characterization. The MGF of NAPGT-II model using the Maclaurin series expansion of an exponential function is mentioned

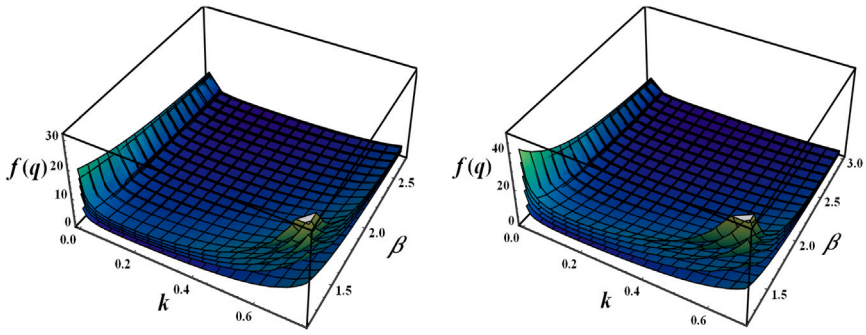

Fig. 4. Variations of quantile density function of NAPGT-II with β and k at different extents of δ with $\lambda = 0.9$ (left), and QF of NAPGT-II with β and k at different extents of δ with $\lambda = 1.9$ (right).

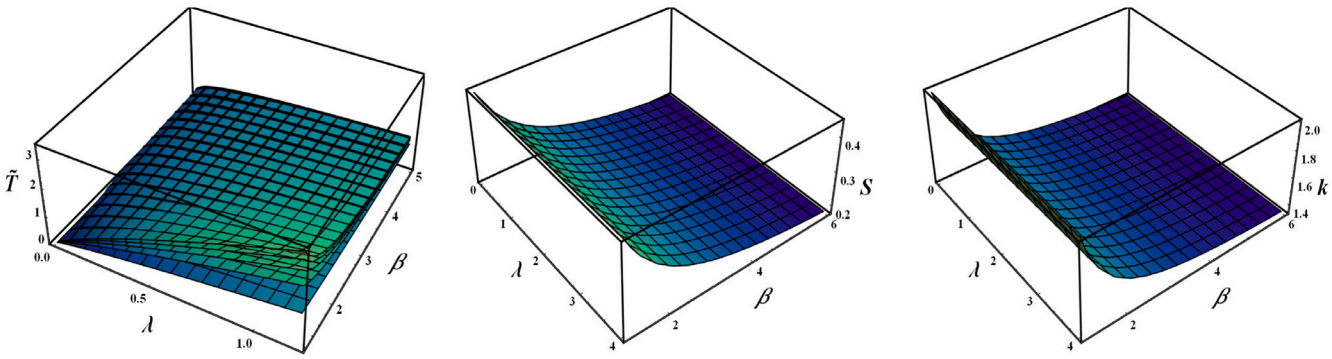

Fig. 5. (i) Fluctuation of $\tilde{T}$ of NAPGT-II with β and at different extents of δ (left) (ii) Fluctuation of skewness (middle) and kurtosis of NAPGT-II at different extents of δ (right).

as

$$M_t(d|\Psi) = E\left(e^{dt}\right) = \sum_{n=0}^{+\infty} \frac{d^n}{n!}\acute{\mu}_n. \tag{28}$$

Stochastic ordering

In this subsection, we compare the NAPGT-II$_1$ $(t|\Psi_1)$ and the NAPGT-II$_2$ $(t|\Psi_2)$ with respect to stochastic ordering information. Assume that T_1 and T_2 be two random variables with reliability functions, cdfs, and pdfs $S_1(t|\Psi_1)$ and $S_2(t|\Psi_2)$; $F_1(t|\Psi_1)$ and $F_2(t|\Psi_2)$; and $f_1(t|\Psi_1)$ and $f_2(t|\Psi_2)$, respectively, where $\Psi_1 = (\delta_1;\beta_1;\lambda_1)$ and $\Psi_2 = (\delta_2;\beta_2;\lambda_2)$ respectively. A random variable $T_1 \leq T_2$ in the following ordering (see [26]), if: (i) Stochastic order $(T_1 \leqslant_{st} T_2)$ if $S_1(t|\Psi_1) \leqslant S_2(t|\Psi_2)$ $\forall\, t$; (ii) Hazard rate order $(T_1 \leqslant_{hr} T_2)$ if $h_1(t|\Psi_1) \geqslant h_2(t|\Psi_2)$ $\forall\, t$; (iii) likelihood ratio order $X \leqslant_{lr} T$ if $\frac{f_{T_1}(t)}{f_{T_2}(t)}$ decreases in t. Among the various partial orderings discussed above, the following chain of implications follows.

$$T_1 \leqslant_{lr} T_2 \Rightarrow T_1 \leqslant_{hr} T_2 \Rightarrow T_1 \leqslant_{st} T_2. \tag{29}$$

As stated in the following theorem, NAPGT-II$(t|\Psi)$ models are ranked according to the strongest "likelihood ratio" ordering.

Theorem 1. *Let* $T_1 \sim NAPGT - II_1(\mu_1;\xi_1;\lambda_1)$, *and* $T_2 \sim NAPGT - II_2(\mu_2;\xi_2;\lambda_2)$, *if* $\beta_1 = \beta_2$, $\lambda_1 = \lambda_2$ *and* $\delta_1 \leq \delta_2$, *then* $T_1 \leqslant_{lr} T_2$ $(T_1 \leqslant_{hr} T_2, T_1 \leqslant_{st} T_2)$ *in all three cases exists.*

Proof. It is sufficient to show $\frac{f_{T_1}(t)}{f_{T_2}(t)}$ is a decreasing function of t; the likelihood ratio is

$$\frac{f_{NAPGT-II_1}(t)}{f_{NAPGT-II_2}(t)} = \frac{\delta_1^{-t^{-\beta}\lambda}\delta_2^{-t^{-\beta}\lambda}}{\log\left[\delta_2\right]}\log\left[\delta_1\right]. \tag{30}$$

Thus if $\beta_1 = \beta_2$, $\lambda_1 = \lambda_2$ and $\delta_1 \leq \delta_2$, then

$$\frac{d}{dt}\left[\frac{f_{NAPGT-II_1}(t)}{f_{NAPGT-II_2}(t)}\right] = \frac{\log\left[\delta_1\right]}{\log\left[\delta_2\right]}\beta\lambda t^{-1-\beta}\delta_1^{-t^{-\beta}\lambda}\delta_2^{-t^{-\beta}\lambda} \times \left(\log\left[\delta_1\right] - \log\left[\delta_2\right]\right) \leq 0. \tag{31}$$

Hence it shows that $T_1 \leqslant_{lr} T_2$, and according to (29) these both are $T_1 \leqslant_{hr} T_2$, $T_1 \leqslant_{st} T_2$ also hold. □

The estimation technique with simulation

In this part, we focus on the MLE technique for estimating NAPGT-II model parameters. Simulation studies are used to investigate the effectiveness of MLE technique. From now, $t_1, t_2, \ldots, t_n$ indicate n observed characteristics from T.

MLE approach

The maximum likelihood strategy is the most extensively used methodology for estimating parameters. Let $T_1, T_2, \ldots, T_n$ be a random sample and the corresponding observed values, $t_1, t_2, \ldots, t_n$ from NAPGT-II model with parameter vector $\Psi = (\lambda, \beta, \delta)$. Then the joint probability function $L(\mathbf{t}|\Psi) = \prod_{i=1}^{n} f(t|\Psi)$ of $T_1, T_2, \ldots, T_n$ as a log-likelihood function is

$$l(\mathbf{t}|\Psi) = \ln\prod_{i=1}^{n} f(t_i;\Psi), \tag{32}$$

$$= n\log(\lambda) + n\log(\beta) - (\beta+1)\sum_{i=1}^{n}\log\left(t_i\right) + n\log\{\log(\delta)\} - \lambda\log(\delta)\sum_{i=1}^{n} t_i^{-\beta} \tag{33}$$

$$\frac{\partial l(\mathbf{t}|\Psi)}{\partial \lambda} = \frac{n}{\lambda} - \log(\delta)\sum_{i=1}^{n} t_i^{-\beta}, \tag{34}$$

$$\frac{\partial l(\mathbf{t}|\Psi)}{\partial \beta} = \frac{n}{\beta} - \sum_{i=1}^{n}\log(t_i) + \lambda\log(\delta)\sum_{i=1}^{n} t_i^{-\beta}\log(t_i), \tag{35}$$

$$\frac{\partial l(\mathbf{t}|\Psi)}{\partial \delta} = \frac{n}{\delta\log(\delta)} - \frac{\lambda}{\delta}\sum_{i=1}^{n} t_i^{-\beta}. \tag{36}$$

The MLEs of the model parameters are achieved by solving the equations above simultaneously. The bias and mean square error of the MLEs, with few exceptions, decrease as sample sizes rise, which fits the common criteria of asymptotic properties of MLEs, according to the simulation study (Section "Numerical and graphical analysis"). In particular, variation in bias and mean square error is observed in all parameter combinations that approaches to zero. Such reflections can be found in Tables 1–4.

Asymptotic confidence bounds

Because the exact magnitude of the parameters cannot be determined, the asymptotic confidence bounds for the unknown parameters of NAPGT-II(λ,β,δ) can be determined using the asymptotic distribution of MLE. We require the information matrix to get these boundaries, which goes like this:

The 2nd partial derivatives of (34–36) are derived by

$$\frac{\partial^2 l(\mathbf{t}|\Psi)}{\partial \lambda^2} = -\frac{n}{\lambda}, \tag{37}$$

$$\frac{\partial^2 l(\mathbf{t}|\Psi)}{\partial \beta^2} = -\frac{n}{\beta^2} - \lambda\log(\delta)\sum_{i=1}^{n} t_i^{-\beta}\left[\log(t_i)\right]^2, \tag{38}$$

$$\frac{\partial^2 l(\mathbf{t}|\Psi)}{\partial \delta^2} = \frac{-n\left[1+\log(\delta)\right]}{\delta^2\left[\log(\delta)\right]^2} + \frac{\lambda}{\delta^2}\sum_{i=1}^{n} t_i^{-\beta}, \tag{39}$$

$$\frac{\partial^2 l(\mathbf{t}|\Psi)}{\partial \lambda\partial \beta} = \log(\delta)\sum_{i=1}^{n}\log(t_i)\, t_i^{-\beta}, \tag{40}$$

$$\frac{\partial^2 l(\mathbf{t}|\Psi)}{\partial \lambda\partial \delta} = -\frac{1}{\delta}\sum_{i=1}^{n} t_i^{-\beta}, \tag{41}$$

$$\frac{\partial^2 l(\mathbf{t}|\Psi)}{\partial \beta\partial \delta} = \frac{\lambda}{\delta}\sum_{i=1}^{n} t_i^{-\beta}\log(t_i). \tag{42}$$

The information matrix is

$$\grave{I} = -\begin{pmatrix} \iota_{11} & \iota_{12} & \iota_{13} \\ \iota_{21} & \iota_{22} & \iota_{23} \\ \iota_{31} & \iota_{32} & \iota_{33} \end{pmatrix}, \tag{43}$$

where $\iota_{11} = E\left(\frac{\partial^2 l(\mathbf{t}|\Psi)}{\partial\lambda^2}\right)$, $\iota_{22} = E\left(\frac{\partial^2 l(\mathbf{t}|\Psi)}{\partial\beta^2}\right)$, $\iota_{33} = E\left(\frac{\partial^2 l(\mathbf{t}|\Psi)}{\partial\delta^2}\right)$, $\iota_{21} = \iota_{12} = E\left(\frac{\partial^2 l(\mathbf{t}|\Psi)}{\partial\lambda\partial\beta}\right)$, $\iota_{13} = \iota_{31} = E\left(\frac{\partial^2 l(\mathbf{t}|\Psi)}{\partial\lambda\partial\delta}\right)$ and $\iota_{23} = \iota_{32} = E\left(\frac{\partial^2 l(\mathbf{t}|\Psi)}{\partial\beta\partial\delta}\right)$. After that, the approximated variance–covariance matrix is:

$$\Omega_{\Psi} = -\begin{pmatrix} \iota_{11} & \iota_{12} & \iota_{13} \\ \iota_{21} & \iota_{22} & \iota_{23} \\ \iota_{31} & \iota_{32} & \iota_{33} \end{pmatrix}^{-1}. \tag{44}$$

In most cases, parameter values are undetermined and must be evaluated using samples; as a result, the expected variance–covariance matrix is specified as

$$\breve{\Omega}_{\breve{\Psi}} = -\begin{pmatrix} \breve{\iota}_{11} & \breve{\iota}_{12} & \breve{\iota}_{13} \\ \breve{\iota}_{21} & \breve{\iota}_{22} & \breve{\iota}_{23} \\ \breve{\iota}_{31} & \breve{\iota}_{32} & \breve{\iota}_{33} \end{pmatrix}^{-1}. \tag{45}$$

Using the above variance–covariance matrix, A$(1-\omega)$100% confidence interval can be constructed for the parameters and stated as

$$\breve{\lambda} \pm Z_{\frac{\omega}{2}}\sqrt{V(\breve{\lambda})}, \breve{\beta} \pm Z_{\frac{\omega}{2}}\sqrt{V(\breve{\beta})}, \breve{\delta} \pm Z_{\frac{\omega}{2}}\sqrt{V(\breve{\delta})} \tag{46}$$

where $Z_{\frac{\omega}{2}}$ is the upper $\left(\frac{\omega}{2}\right)$ th percentile of the SND.

Numerical and graphical analysis

The ML estimators of the NAPGT-II model are not in closed form, as shown in the prior section. As a result, a simulation experiment is conducted to assess the trend of estimates utilizing various metrics such as mean square errors (MSEs), root mean square error (RMSE) and average bias (AB) values, and also their asymptotic behavior for finite samples.

To evaluate the finite sample behavior of MLEs, we can perform simulation experiments numerically and graphically. The decision has been made using the given algorithm:

1. Generate a thousand samples of size n from (6). QF accomplished all of the work and gleaned the data from a uniform distribution.

2. Exact values of different combinations of the model parameters λ,β and δ are considered as set -I: $(0.7, 0.9, 1.5)$, set -II: $(1.1, 1.3, 1.2)$,set -III: $(1.2, 1.4, 1.2)$ and set -IV: $(2.1, 0.25, 1.15)$.

3. Compute the estimates for 1000 samples, say $\left(\hat{\lambda}_k, \hat{\beta}_k, \hat{\delta}_k\right)$ for $k = 1, 2, \ldots, 1000$.

4. Appraise average bias (AB) value, MSEs and RMSE. These targets are acquired with following formulas:

$$Bias_{\Psi}(n) = \frac{1}{1000}\sum_{i=1}^{1000}\left(\breve{\Psi}_i - \Psi\right), \tag{47}$$

$$MSE_{\Psi}(n) = \frac{1}{1000}\sum_{i=1}^{1000}\left(\breve{\Psi}_i - \Psi\right)^2, \tag{48}$$

$$RMSE_{\Psi}(n) = \sqrt{\frac{1}{1000}\sum_{i=1}^{1000}\left(\breve{\Psi}_i - \Psi\right)^2}. \tag{49}$$

where $\Psi = (\lambda,\beta,\delta)$.

5. These processes have been replicated with the defined parameters for MLEs for $n = 30, 35, \ldots, 500$. The bias $_{\psi}(n)$ and MSE$_{\psi}(n)$ have both been computed. We utilized optim function of R to assess the quality of estimates. Tables 1–4 and Figs. 6–9 illustrate the findings of the simulations. These ABs and MSEs fluctuate with respect to n in Figs. 6–9 (left panels and right panels).

Because as n increases, the bias approaches zero, we may infer that estimators exhibit the attribute of asymptotic unbiasedness. Meanwhile, the trend in the MSE indicates consistency because the error approaches zero as n rises.

Conclusions on the Simulation Results

The outcomes of the study are interpreted through graphs and tables as described in the results and discussion. The main findings of study can be stated as follows:

- Tables 1–4 show the AB, MSE, and RMSE values of the parameters for various sample sizes and it is noticed that MSE, RMSE decreases as the sample size increases, as expected. Furthermore, as sample size increases, so does the AB.
- The biases of $\hat{\lambda}$ $\hat{\beta}$ and $\hat{\delta}$ decrease as n rises.
- The biases of $\hat{\lambda}$ and $\hat{\beta}$ are relatively positive, however there exist few negative biases for $\hat{\delta}$.
- The MLEs of $\hat{\lambda}$ and $\hat{\beta}$ are overestimated however, MLEs of $\hat{\delta}$ are underestimated (see left panel of Figs. 6 and 9).
- As shown in right panel of Figs. 6–9, the maximum likelihood technique of estimation outperforms in terms of MSE (check right panel of Figs. 6–9).
- According to Figs. 6–9, when the n grows, all bias and MSE plots for all parameters eventually reach zero. That highlights the accuracy of estimation techniques.
- Based on these results, we draw the conclusion that MLEs do a good job of estimating parameters and that the estimates seem to be reasonably constant and closer to the true values for these sample sizes. These findings demonstrate the MLEs' efficiency as well as their consistency.

Table 1
Average values of Biases and MSEs values of MLEs from Simulation of the NAPGT-II distribution for $(\lambda = 0.7, \beta = 0.9, \delta = 1.5)$.

n	30	50	80	140	200	260	320	500
AB $(\hat{\lambda})$	0.4932	0.3352	0.1529	0.0729	0.0561	0.0534	0.05100	0.0467
MSE $(\hat{\lambda})$	0.3068	0.1580	0.0489	0.0113	0.0084	0.0079	0.0073	0.0071
RMSE $(\hat{\lambda})$	0.5539	0.3975	0.2211	0.1063	0.0917	0.0889	0.0854	0.0843
AB $(\hat{\beta})$	0.0417	0.03341	0.1064	0.0969	0.0966	0.0895	0.0973	0.0939
MSE $(\hat{\beta})$	0.2165	0.1479	0.0312	0.0149	0.0139	0.0134	0.0115	0.0109
RMSE $(\hat{\beta})$	0.4653	0.3846	0.1766	0.1221	0.1179	0.1158	0.1072	0.1044
AB $(\hat{\delta})$	−0.0206	−0.0759	0.0410	0.0254	0.0066	0.0030	0.0006	0.0002
MSE $(\hat{\delta})$	0.0105	0.0245	0.0063	0.0061	0.0058	0.0053	0.0049	0.0044
RMSE $(\hat{\delta})$	0.1025	0.1565	0.0794	0.0781	0.0762	0.0728	0.0700	0.0663

Table 2
Average values of Biases and MSEs values of MLEs from Simulation of the NAPGT-II distribution for $(\lambda = 1.1, \beta = 1.3, \delta = 1.2)$.

n	30	50	80	140	200	260	320	500
AB $(\hat{\lambda})$	0.2306	0.0792	0.0424	0.0365	0.0307	0.0270	0.0254	0.0247
MSE $(\hat{\lambda})$	0.0847	0.0143	0.0055	0.0047	0.0045	0.0042	0.0039	0.0031
RMSE $(\hat{\lambda})$	0.2910	0.1196	0.0742	0.0686	0.0671	0.0648	0.0625	0.0557
AB $(\hat{\beta})$	0.3365	0.0719	0.0475	0.0475	0.0512	0.0538	0.0565	0.0583
MSE $(\hat{\beta})$	0.1586	0.0185	0.0105	0.0059	0.0056	0.0053	0.0052	0.0049
RMSE $(\hat{\beta})$	0.3983	0.1360	0.1025	0.0768	0.0748	0.0728	0.0721	0.0700
AB $(\hat{\delta})$	0.3263	0.0860	0.0481	0.0459	0.0415	0.0387	0.0355	0.0347
MSE $(\hat{\delta})$	0.2003	0.0240	0.0062	0.0059	0.0056	0.0050	0.0048	0.0045
RMSE $(\hat{\delta})$	0.4476	0.1549	0.0787	0.0768	0.0748	0.0707	0.0693	0.0671

Table 3
Average values of Biases and MSEs values of MLEs from Simulation of the NAPGT-II distribution for $(\lambda = 1.2, \beta = 1.4, \delta = 1.2)$.

n	30	50	80	140	200	260	320	500
AB $(\hat{\lambda})$	0.1382	0.0490	0.0351	0.0285	0.0240	0.0210	0.0191	0.0175
MSE $(\hat{\lambda})$	0.0413	0.0069	0.0049	0.0044	0.0034	0.0032	0.0030	0.0024
RMSE $(\hat{\lambda})$	0.2032	0.0831	0.0700	0.0663	0.0583	0.0566	0.0548	0.0489
AB $(\hat{\beta})$	0.1869	0.0245	0.0385	0.0350	0.0315	0.0295	0.0245	0.0105
MSE $(\hat{\beta})$	0.0562	0.0049	0.0054	0.0049	0.0044	0.0039	0.0034	0.0030
RMSE $(\hat{\beta})$	0.0237	0.0700	0.0735	0.0700	0.0663	0.0624	0.0583	0.0548
AB $(\hat{\delta})$	0.2424	0.0665	0.0890	0.0875	0.0845	0.0775	0.0762	0.0752
MSE $(\hat{\delta})$	0.1264	0.0093	0.0113	0.0103	0.0137	0.0124	0.0117	0.0109
RMSE $(\hat{\delta})$	0.3555	0.0964	0.1063	0.1015	0.1171	0.1114	0.1082	0.1044

Table 4
Average values of Biases and MSEs values of MLEs from Simulation of the NAPGT-II distribution for $(\lambda = 2.1, \beta = 0.25, \delta = 1.15)$.

n	30	50	80	140	200	260	320	500
AB $(\hat{\lambda})$	−0.1676	−0.0975	−0.0568	−0.0164	−0.0031	0.0000	0.0000	0.0000
MSE $(\hat{\lambda})$	0.0473	0.0196	0.0087	0.0024	0.0006	0.0001	0.0000	0.0000
RMSE $(\hat{\lambda})$	0.2175	0.1400	0.0933	0.0490	0.0245	0.0100	0.0000	0.0000
AB $(\hat{\beta})$	0.3370	0.2689	0.2502	0.2500	0.2499	0.2021	0.0453	0.0012
MSE $(\hat{\beta})$	0.1214	0.0768	0.0679	0.0625	0.0623	0.0612	0.0603	0.0600
RMSE $(\hat{\beta})$	0.3484	0.2771	0.2606	0.2500	0.2496	0.2474	0.2456	0.2450
AB $(\hat{\delta})$	0.2591	0.1833	0.1213	0.0773	0.0341	0.0072	0.0000	0.0000
MSE $(\hat{\delta})$	0.1016	0.0579	0.0214	0.0095	0.0021	0.0000	0.0000	0.0000
RMSE $(\hat{\delta})$	0.3187	0.2406	0.1463	0.0975	0.0458	0.0000	0.0000	0.0000

Real data practices

In this portion, the NAPGT-II model's usefulness for two real data sets is presented. The NAPE (New Alpha Power Exponential) model [21], EGT-II (Exponentiated Gumbel Type-II) [27], Weibull, Gumbel Type-Two (GT-II) and Exponentiated Generalized Gumbel Type-II (EGGT-II) [28] Distribution are all considered viable alternatives to the NAPGT-II model. The analytical measures Kolmogorov–Smirnov (K-S) statistic and its *P*-value (PV) have been used to compare these models. The model with the lowest analytical measures scores for the real data set with the highest PV may be the best fit. The results of these examinations are shown in Tables 5 and 6.

The first data represents COVID-19 data represent the daily new deaths which belong to Argentina in 65 days recorded from 1 June to 4 August 2020, second real data collection presented COVID-19 data from Italy, which spans 35 days from April 1 to May 5, 2020 and is available at [https://covid19.who.int/]. This data is calculated by dividing daily new deaths by new cases. The detail of this dataset can be seen in Hassan et al. [29]. See [30–33] for other examples of COVID-19 data applications. To assess the pertinent parameters of models, the MLE method has been utilized. Tables 5 and 6 provide ML estimates and their standard errors (SEs) in parenthesis, for two real data sets. The results in these tables prove that proposed distribution gives better fits than competing models, as NAPGT model has the highest P-value and the smallest Kolmogorov–Smirnov (K-S) distance. The fitted PDF, CDF and P-P layouts of the NAPGT-II distribution for the two real data sets are depicted, respectively, in Figs. 10 and 11. These figures support the values in Tables 5 and 6, that the NAPGT-II distribution provides close fit for the two real data sets. Figs. 12 and 14 provide profile-likelihood plots of the NAPGT-II parameters for the two real data sets. These plots illustrate the unimodality of profile-likelihood functions for all estimated parameters. The existence and uniqueness of

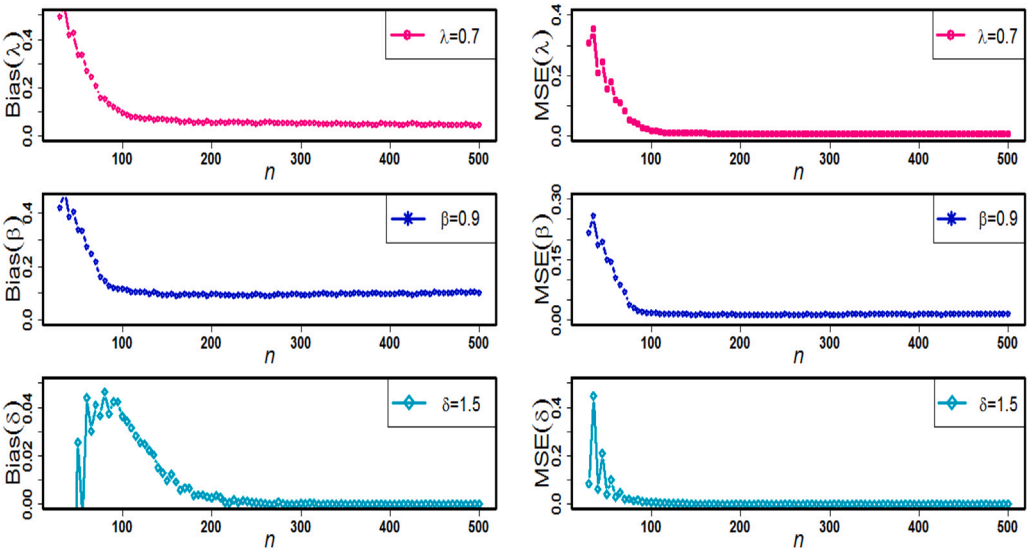

Fig. 6. Variation of Bias and MSE of $\hat{\lambda}, \hat{\beta}$ and $\hat{\delta}$.

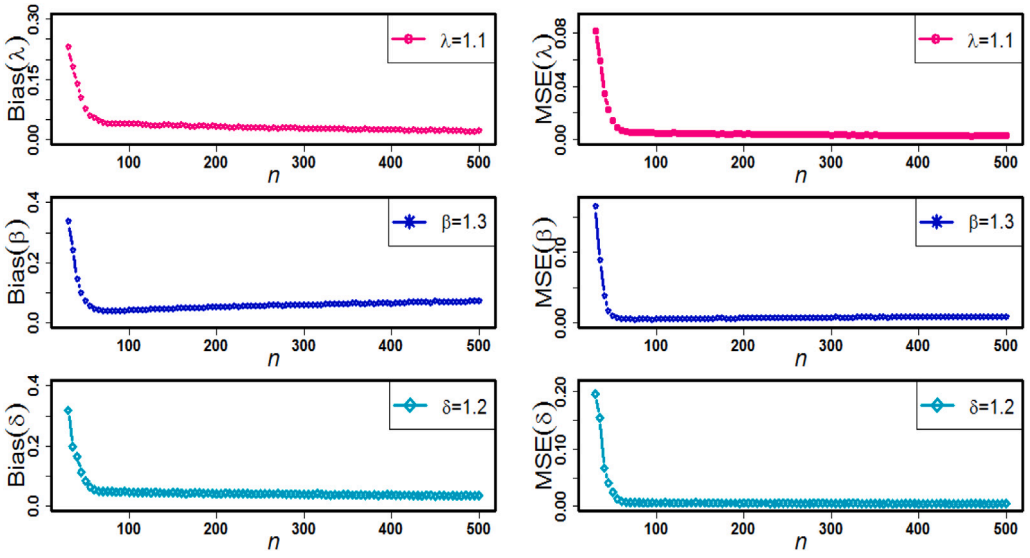

Fig. 7. Variation of Bias and MSE of $\hat{\lambda}, \hat{\beta}$ and $\hat{\delta}$.

Table 5
MLEs, SEs of the parameters and K-S statistic with *P*-value of considered models for data Set I.

Models	MLEs	Standard errors	K-S	*P*-value
NAPE $(\check{\lambda}, \check{\xi})$	19.7022, 0.03801	4.7161, 0.0034	0.1224	0.2848
NAPGT-II $(\check{\lambda}, \check{\beta}, \check{\delta})$	118.0960, 1.6728, 9.8709	3.6130, 0.000, 2.966	0.0804	0.7944
EGT-II $(\check{\xi}, \check{\beta}, \check{\kappa})$	5.2947, 0.7958, 37.9722	5.6157, 0.3264, 26.7375	0.9902	0.0000
Weibull $(\check{\vartheta}, \check{\kappa})$	1.5567, 54.5182	0.1423, 4.6119	0.1472	0.1197
EGGT-II	0.0703, 6.8688,	0.0031, 1.0901,	0.4414	0.0000
	6.5774, 200.6077	0.0029, 24.8823	0.2537	0.0179

estimated parameters for the proposed model are shown graphically in Figs. 13 and 15, respectively, for the two real data sets. Finally, NAPGT-II model emerges as the most appropriate model for both datasets, demonstrating its usefulness in a real context.

Closing remarks on both applications

1. NAPGT-II has the highest *P*-value and the lowest K-S distance, according to both datasets.

2. As shown in Figs. 10 and 11 NAPGT-II is the most effective model for fitting datasets I and II.

3. The EGT-II and EGGT-II distributions demonstrate poor fit for the first dataset, as shown in Table 5.

4. The NAPE and GT-II models demonstrate poor fit for the second dataset, as shown in Table 6.

5. The existence and uniqueness of estimated parameters for the proposed model can be noticed in Figs. 13 and 15, respectively, for the two real data sets.

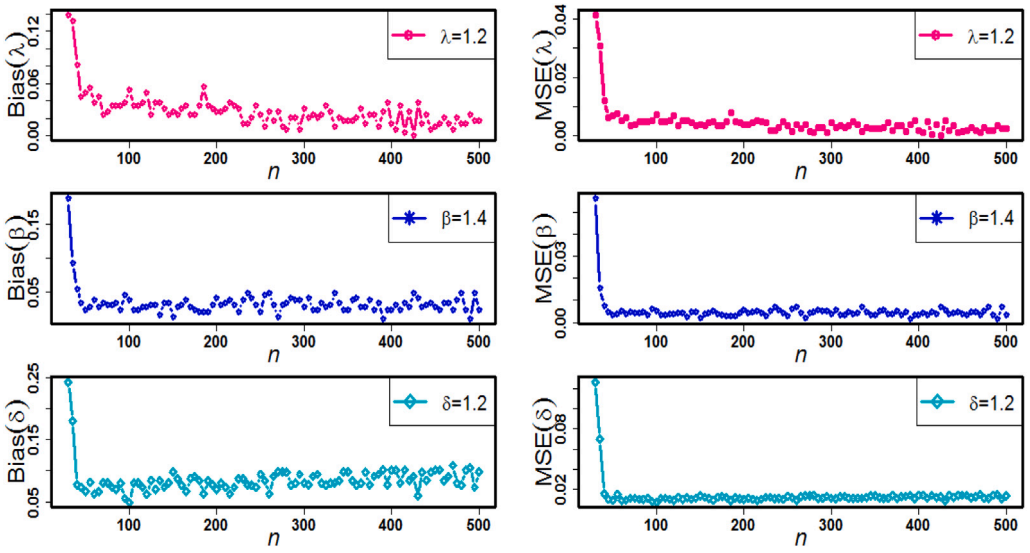

Fig. 8. Variation of Bias and MSE of $\hat{\lambda}, \hat{\beta}$ and $\hat{\delta}$.

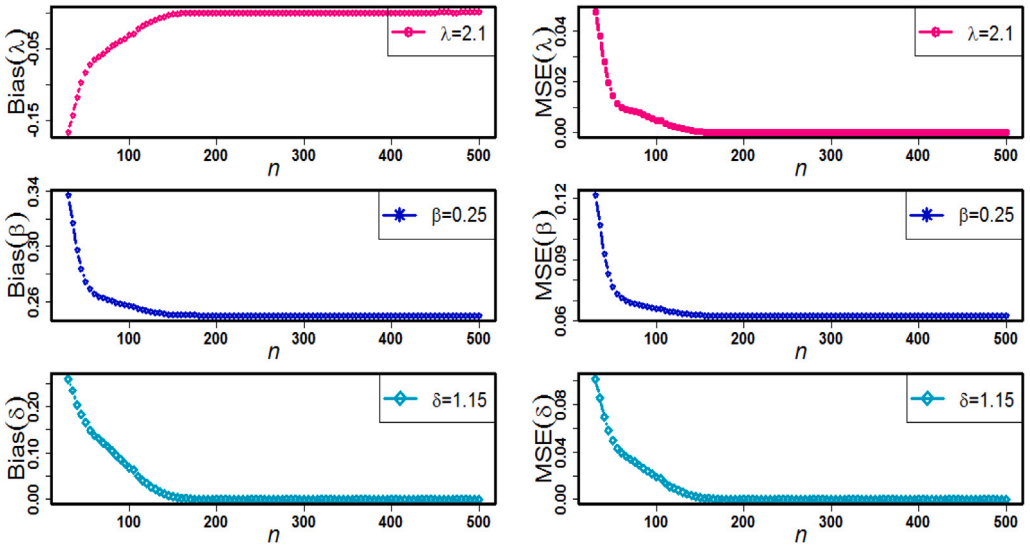

Fig. 9. Variation of Bias and MSE of $\hat{\lambda}, \hat{\beta}$ and $\hat{\delta}$.

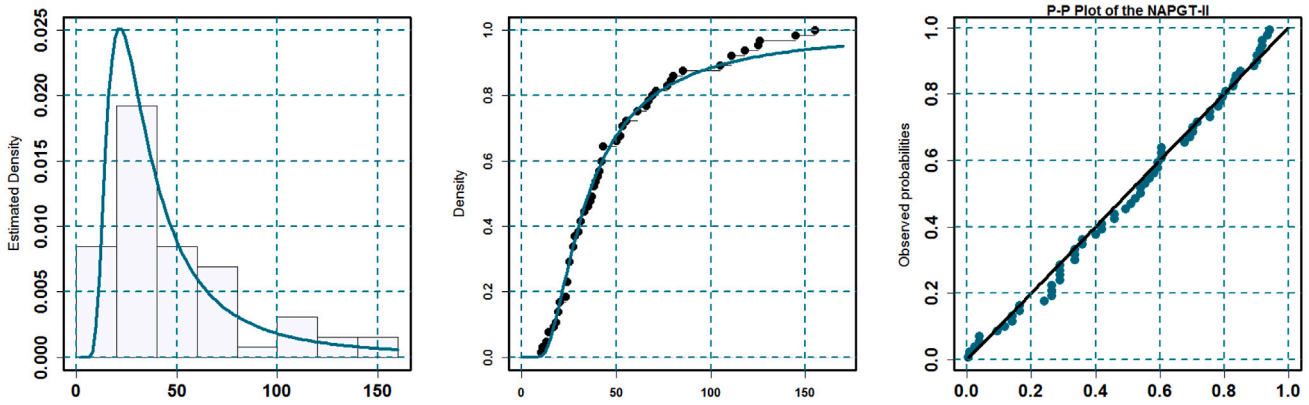

Fig. 10. Fitted density plotted over the sample histogram of dataset I (left panel), fitted CDFs on empirical CDF (middle panel) and P-P layouts of dataset I (right panel).

Table 6
MLEs, SEs of the parameters and K-S statistic with P-value of considered models for data Set II.

Models	MLEs	Standard errors	K-S	P-value
NAPE $(\check{\lambda}, \check{\xi})$	135.5089, 13.2114	79.5693, 1.3148	0.2788	0.0068
NAPGT-II $(\check{\lambda}, \check{\beta}, \check{\delta})$	0.0063, 5.2431, 1.0064	0.0043, 0.4208, 0.0044	0.0889	0.9217
EGT-II $(\check{\xi}, \check{\beta}, \check{\kappa})$	6.4945, 2.4718, 0.0238	4.0462, 0.5118, 0.0282	0.9891	0.0000
Weibull $(\check{\vartheta}, \check{\kappa})$	5.2152, 0.1750	0.6407, 0.0060	0.1102	0.7480
GT-II $(\check{\beta}, \check{\kappa})$	0.0025, 3.1696	0.0006, 0.1391	0.2537	0.0179

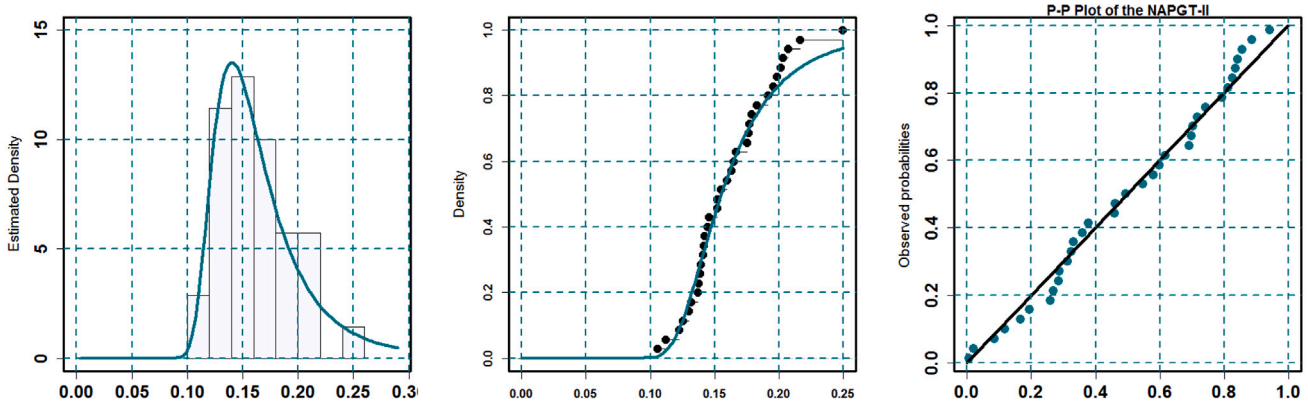

Fig. 11. Fitted density plotted over the sample histogram of dataset I (left panel). fitted CDFs on empirical CDF (middle panel) and P-P layouts of dataset II (right panel).

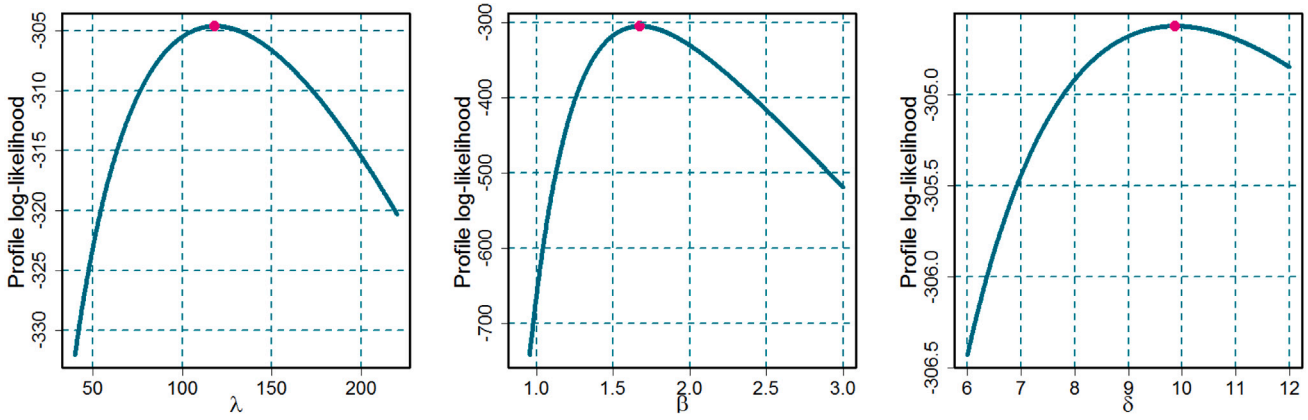

Fig. 12. Plots of the profile-likelihood functions for the two estimated parameters of the first real data set.

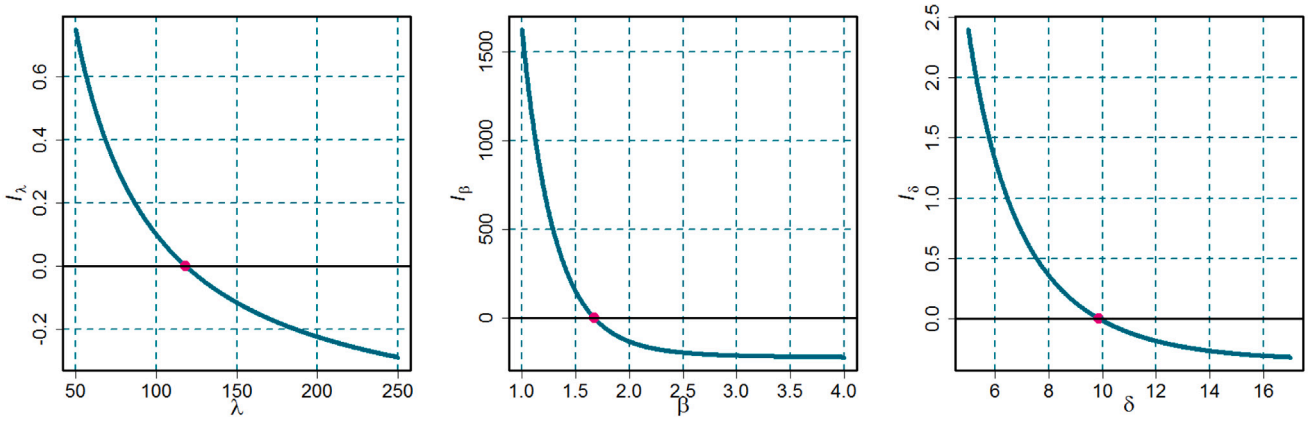

Fig. 13. Existence and uniqueness of NAPGT-II parameters λ, β and δ for dataset I.

Concluding remarks

The three-parameter new alpha power Gumbel Type II (NAPGT-II) model is proposed in this study. The NAPGT-II model is more adaptable than other known models when it comes to studying lifespan data. This is a brief summary of what we are trying to accomplish. The estimation methodologies like MLE is employed to evaluate the parameters of NAPGT-II model. A emulation study is used to assess the

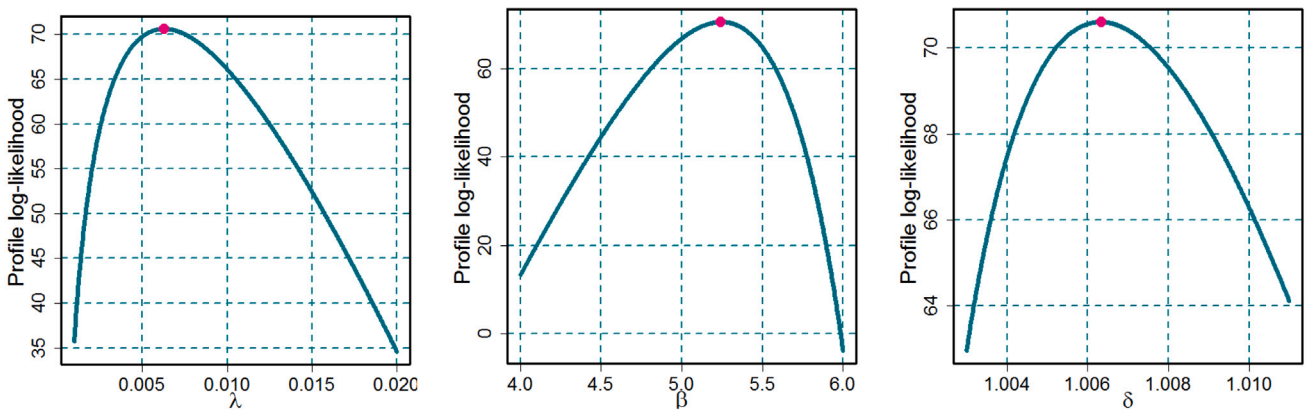

Fig. 14. Plots of the profile-likelihood functions for the two estimated parameters of the second real data set.

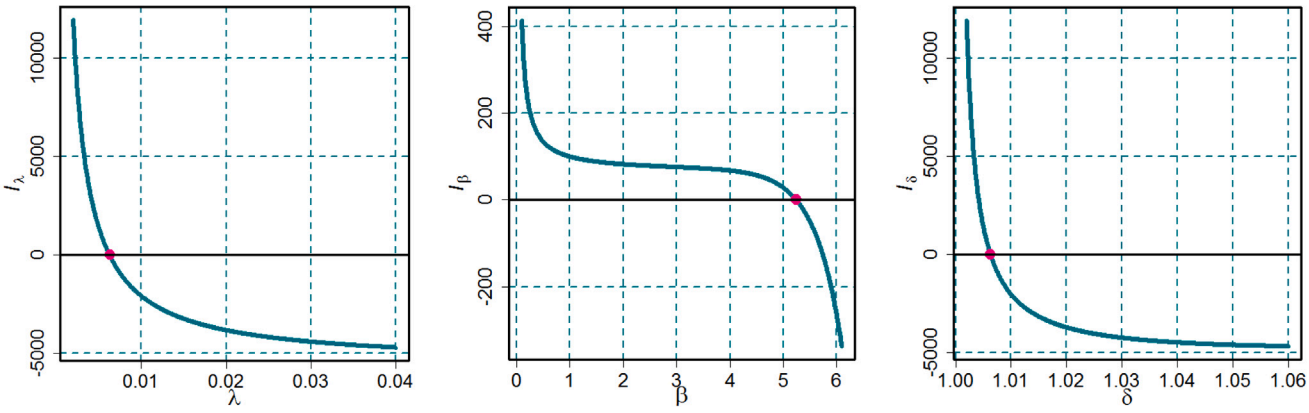

Fig. 15. Existence and uniqueness of NAPGT-II parameters λ, β and δ for dataset II.

model's performance under several sample sizes and several values of the parameters. We represent two accomplishment based on the COVID 19 mortality rate. We concluded that it had the lowest K-S and the highest P-values, making it the best choice among all its competitors. Additionally, to ensure that the roots of the proposed distribution's MLE offer a maximum value, we graphed Figs. 12 and 14 for the profile-likelihood function of the proposed model with its parameters for the real data set. These plots demonstrate the unimodality of all calculated parameters' profile-likelihood functions.

Nomenclature

Symbols

$f(t\|\Psi)$	PDF	$F(t\|\Psi)$	CDF
$S(t\|\Psi)$	SF	$h(t\|\Psi)$	HRF/FRF
$H(t\|\Psi)$	CHRF	$t(k\|\Psi)$	QF
$t'(k\|\Psi)$	Quantile Density Function	$M_t(d\|\Psi)$	MGF
$\hat{\Omega}_{\hat{\Psi}}$	Variance–Covariance		

Abbreviations

MLE	Maximum likelihood Estimation	EGT-II	Exponentiated Gumbel Type-II
GT-II	Gumbel Type II	NAPGT-II	New Alpha Power Gumbel Type II
PDF	Probability Density Function	FGF	Factorial Generating Function
SND	Standard Normal Distribution	CHRF	Cumulative Hazard Rate Function
SF	Survival Function	FRF	Failure Rate Function
hrf	hazard rate function	RMSE	Root Mean Square Error
AB	Average Bias	MSE	Mean square error
EGGT-II	Exponentiated Generalized Gumbel Type-II	CDF	Cumulative Distribution Function
MGF	Moment Generating Function	QF	Quantile Function
ED	Exponential distribution		

Declaration of competing interest

The authors declare that they have no known competing financial interests or personal relationships that could have appeared to influence the work reported in this paper.

Data availability

All data generated or analyzed during this study are included in this article.

References

[1] Weibull W. A statistical distribution function of wide applicability. J Appl Mech 1951;18(3):293–7.
[2] Aldeni M, Lee C, Famoye F. Families of distributions arising from the quantile of generalized lambda distribution. J Stat Distributions Appl 2017;4(1):1–18.
[3] Alzaatreh A, Lee C, Famoye F. T-normal family of distributions: a new approach to generalize the normal distribution. J Stat Distributions Appl 2014;1(1):1–18.
[4] Cordeiro GM, Alizadeh M, Ramires TG, Ortega EM. The generalized odd half-Cauchy family of distributions: properties and applications. Comm Statist Theory Methods 2017;46(11):5685–705.
[5] Eugene N, Lee C, Famoye F. Beta-normal distribution and its applications. Comm Statist Theory Methods 2002;31(4):497–512.
[6] Jones MC. Kumaraswamy's distribution: A beta-type distribution with some tractability advantages. Stat Methodol 2009;6(1):70–81.

[7] Mahdavi A, Kundu D. A new method for generating distributions with an application to exponential distribution. Comm Statist Theory Methods 2017;46(13):6543–57.
[8] Nassar M, Alzaatreh A, Mead M, Abo-Kasem O. Alpha power Weibull distribution: Properties and applications. Comm Statist Theory Methods 2017;46(20):10236–52.
[9] Ramadan DA, Magdy W. On the alpha-power inverse Weibull distribution. Int J Comput Appl 2018;181(11):6–12.
[10] Dey S, Alzaatreh A, Zhang C, Kumar D. A new extension of generalized exponential distribution with application to ozone data. Ozone: Sci Eng 2017;39(4):273–85.
[11] Dey S, Nassar M, Kumar D. Alpha power transformed inverse Lindley distribution: A distribution with an upside-down bathtub-shaped hazard function. J Comput Appl Math 2019;348:130–45.
[12] Dey S, Ghosh I, Kumar D. Alpha-power transformed Lindley distribution: properties and associated inference with application to earthquake data. Ann Data Sci 2019;6(4):623–50.
[13] Ihtisham S, Khalil A, Manzoor S, Khan S, Ali A. Alpha-power Pareto distribution: Its properties and applications. PLoS One 2019;14(6):e0218027.
[14] Ijaz M, Asim SM, Farooq M, Khan SA, Manzoor S. A gull alpha power Weibull distribution with applications to real and simulated data. Plos One 2020;15(6):e0233080.
[15] de Brito E, Silva GO, Cordeiro GM, Demétrio CGB. The mcdonald gumbel model. Comm Statist Theory Methods 2016;45(11):3367–82.
[16] Gupta J, Garg M, Gupta M. The Lomax-Gumbel distribution. Palest J Math 2016;5(1):35–42.
[17] Gholami G, Pourdarvish A, MirMostafaee SMT, Alizadeh M, Nashi AN. On the Gamma Gumbel distribution. Appl Math E-Notes 2020;20:142–54.
[18] Cordeiro GM, Nadarajah S, Ortega EM. The Kumaraswamy Gumbel distribution. Stat Methods Appl 2012;21(2):139–68.
[19] Nadarajah S, Kotz S. The beta Gumbel distribution. Math Probl Eng 2004;2004(4):323–32.
[20] Sindhu TN, Shafiq A, Al-Mdallal QM. Exponentiated transformation of Gumbel Type-II distribution for modeling COVID-19 data. Alex Eng J 2021;60(1):671–89.
[21] Ijaz M, Mashwani WK, Göktaş A, Unvan YA. A novel alpha power transformed exponential distribution with real-life applications. J Appl Stat 2021;48(11):I–XVI.
[22] Kundu D, Raqab MZ. Generalized Rayleigh distribution: different methods of estimations. Comput Statist Data Anal 2005;49(1):187–200.
[23] Mazucheli J, Louzada F, Ghitany ME. Comparison of estimation methods for the parameters of the weighted Lindley distribution. Appl Math Comput 2013;220:463–71.
[24] Sindhu TN, Saleem M, Aslam M. Bayesian Estimation for Topp Leone distribution under trimmed samples. J Basic Appl Sci Res 2013;3(10):347–60.
[25] Hyndman RJ, Fan Y. Sample quantiles in statistical packages. Amer Statist 1996;50(4):361–5.
[26] Shaked M. Shanthikumar. In: JG Stochastic Orders. Springer; 2007.
[27] Okorie IE, Akpanta AC, Ohakwe J. The exponentiated Gumbel type-2 distribution: properties and application. Int J Math Math Sci 2016;2016.
[28] Ogunde AA, Fayose ST, Ajayi B, Omosigho DO. Extended Gumbel type-2 distribution: properties and applications. J Appl Math 2020;2020.
[29] Hassan AS, Almetwally EM, Ibrahim GM. Kumaraswamy inverted topp–leone distribution with applications to COVID-19 data. CMC-Comput Mat Continua 2021;68(1):337–58.
[30] Abu El Azm WS, Almetwally EM, Naji AL-Aziz S, El-Bagoury AAAH, Alharbi R, Abo-Kasem OE. A new transmuted generalized lomax distribution: Properties and applications to COVID-19 data. Comput Intell Neurosci 2021;2021.
[31] Shafiq A, Lone SA, Sindhu TN, El Khatib Y, Al-Mdallal QM, Muhammad T. A new modified Kies Fréchet distribution: Applications of mortality rate of Covid-19. Results Phys 2021;28:104638.
[32] Lone SA, Sindhu TN, Jarad F. Additive Trinomial Fréchet distribution with practical application. Results Phys 2021;105087.
[33] Sindhu TN, Shafiq A, Al-Mdallal QM. On the analysis of number of deaths due to Covid- 19 outbreak data using a new class of distributions. Results Phys 2021;21:103747.